Magnetization steps and relevant cluster statistics for a diluted Heisenberg layer: Nearest-neighbor cluster model on the square lattice

Valdir Bindilatti*
Instituto de Física, Universidade de São Paulo, Caixa Postal 66.318, 05315–970 São Paulo-SP, Brazil

Yaacov Shapira†
Department of Physics and Astronomy, Tufts University, Medford, Massachusetts 02155, USA
(Received 3 February 2005; published 8 August 2005)

A theory for magnetization steps (MST's) from a strongly diluted Heisenberg antiferromagnet on the square lattice will be presented in several papers. In this first paper, general results for cluster models are reviewed, including an updated in-depth discussion of cluster types. A detailed equilibrium theory for the nearest-neighbor (NN) cluster model on the square lattice is then presented. The fraction x of cations that are magnetic is assumed to be well below the site percolation concentration, $x_c=0.593$ for this model. Isotropic exchange interactions (Heisenberg exchange) are the only intracluster interactions. Neighbors are classified by symmetry, instead of the traditional classification by the distance r. Neighbors in the same symmetry class have the same isotropic exchange constant J, so that the J's too can be classified by these symmetry classes. For the square lattice, twelve of the neighbors' symmetry classes correspond to the twelve shortest r's. The corresponding J's are as follows: J_1 for NN's, J_2 for second neighbors, and so on up to J_{12}. Clusters are divided into "types." Each type, c, is specified by the cluster size n_c (the number of spins), and by a "bond list" that specifies the J's for all spin pairs in the cluster. The bond list determines the cluster's exchange Hamiltonian. The relevant statistics is therefore the statistics of cluster types, not of cluster sizes. The main assumption in the statistics is that the magnetic ions are randomly distributed over all cation sites. For the NN cluster model on the square lattice, there are 3290 cluster types with sizes $n_c \leqslant 12$. Perimeter polynomials (PP's) for cluster types, analogous to the usual PP's for cluster sizes, are given for all 3290 cluster types. The energy eigenvalues for the 10 cluster types with sizes $n_c \leqslant 5$ were determined for magnetic ions with spin $S=5/2$, such as Mn^{2+} and Fe^{3+}. The average magnetic moment $\mu_c(T,B)$ per cluster, for these 10 cluster types, was then obtained at temperature T and magnetic field B. At low T, all cluster types with sizes $n_c>1$ give rise to MST's. The total magnetization M is proportional to a statistically-weighted average of $\mu_c(T,B)$ over all cluster types. The contribution from cluster types with $n_c \leqslant 5$ is dominant when $x \leqslant 0.25$. This contribution is evaluated exactly. Two alternative approximations are used to evaluate the contribution from the larger clusters. Examples of calculated magnetization curves are given. In addition to the MST's, the magnetization exhibits a fast rise at low B. This rise ends in a plateau (the plateau of "apparent saturation"). The apparent saturation value M_s is calculated for x up to 0.25. This paper is accompanied by electronically accessible tables (EPAPS) of numerical results for all 3290 cluster types.

DOI: 10.1103/PhysRevB.72.064414 PACS number(s): 75.10.Jm, 75.10.Nr, 75.50.Ee, 05.50.+q

I. INTRODUCTION

The magnetization-step (MST) method is among the most powerful for studying small clusters of magnetic ions. Predicted theoretically long ago,[1] MST's were used to study diluted magnetic semiconductors.[2] The method has been later extended to the study of clusters in diluted magnetic insulators, and in molecular crystals.[3,4] The information that has been obtained with the MST method includes (1) antiferromagnetic (AF) exchange constants, (2) magnetic-anisotropy parameters, and (3) the distribution of the magnetic ions in diluted magnetic materials.

Many studies of MST's were carried out under the conditions of thermal equilibrium. However, nonequilibrium behavior was also studied extensively in connection with macroscopic quantum tunneling of the magnetization.[5–7] Nonequilibrium behavior was also observed in pulsed magnetic fields of milliseconds duration.[8]

Nearly all previous MST studies in diluted magnetic materials focused on AF clusters in three dimensional (3D) solids. One exception is a recent study of a diluted Heisenberg AF chain (1D).[8] Another is a study by Crooker *et al.* of quasi-2D heterostructures.[9]

The present paper is the first of several theoretical and experimental papers on MST's from a strongly diluted AF layer (2D). Following a review of the general theoretical framework (with several important new additions), the nearest-neighbor (NN) cluster model on the square lattice is treated in detail. Extensive results for the relevant cluster statistics, for clusters with up to 12 spins, are given. The exact average magnetic moment for clusters with up to 5 spins is obtained from the energy eigenvalues. Larger clusters are treated approximately. The results for small and large clusters are combined to produce examples of magnetization curves.

The present paper is already adequate for interpreting those experimental data in the following paper[10] that were obtained at 0.6 K. These MST data are for AF layers with the chemical formula $(C_3NH_3)_2Mn_xCd_{1-x}Cl_4$. The thermal

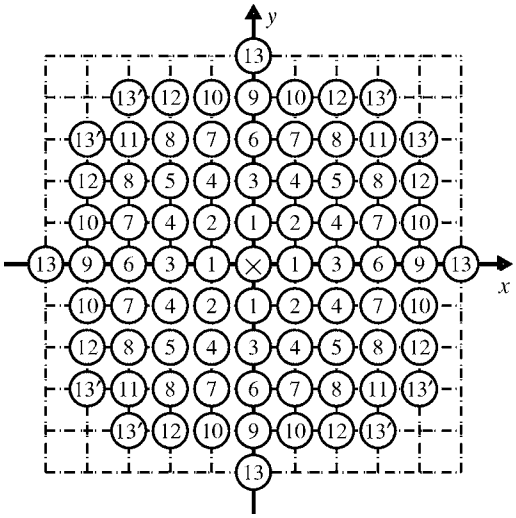

FIG. 1. Lattice sites on the square lattice. The central site is marked by "×." Other sites are divided into numbered symmetry classes.

broadening at 0.6 K obscured the fine structure due to weak interactions that are neglected in the present paper. The interpretation of the fine structure that was observed in the same samples at temperatures of order 10 mK is based on other theoretical results.

Background material for the present paper may be found in a recent review.[3] As in this review, the theory presented here is an equilibrium theory. That is, the sample is both in internal equilibrium and in thermal equilibrium with its surroundings.

II. CLUSTER MODELS

Cluster models are indispensable for treating MST's in diluted magnetic materials. Here, relevant aspects of these models are summarized, and selected topics are discussed in greater detail than in earlier works, including Ref. 3. The added details are essential for the presentation.

A. Classification of neighbors on the square lattice

Figure 1 shows the square lattice. The locations of the lattice sites can be specified by using an x-y coordinate system in which the unit length is the lattice parameter a. The lattice sites correspond to the positions of the cations (both magnetic and nonmagnetic) in the diluted magnetic layer. The cation at the origin, marked by "×," is the "central" cation. Any other cation is a "neighbor" of the central cation.

The neighbors in Fig. 1 are classified by symmetry. Neighbors in the same symmetry class occupy equivalent position in the cation lattice. The traditional classification of neighbors is based on the distance r from the central site, not on symmetry. It is useful to compare the two classifications. The symmetry classes that are numbered as 1 up to 12 in Fig. 1 correspond to the 1st up to the 12th neighbors, respectively, in the classification by distance. This simple correspondence between symmetry and distance stops at the 13th neighbors. All the 13th neighbors are at a distance $r=5a$, but they belong to two different symmetry classes, labeled in the figure as 13 and 13′. Symmetry class No. 13 consists of four neighbors at $(x,y)=(0,\pm5),(\pm5,0)$, while symmetry class No. 13′ consists of eight neighbors at $(\pm3,\pm4)$, $(\pm4,\pm3)$. Other examples of equidistant but symmetry-inequivalent neighbors are the 24th, 30th, 38th, and 43rd neighbors. There are no other examples up to the 50th neighbors.

The division of neighbors into symmetry classes has been discussed in Refs. 3,11. These symmetry classes are particularly useful in discussions of isotropic exchange interactions between identical magnetic ions. When these magnetic ions (spins) are placed on cation sites, the isotropic exchange constant J between the central spin and any spin in the same symmetry class is the same. Except for accidental degeneracy, exchange constants with neighbors in different symmetry classes are different. For example, the neighbors labeled as 13 and 13′ in Fig. 1 are expected to have different exchange constants. (The difference in this case is not likely to be of great practical importance, however, because exchange interactions with neighbors more distant than the 12th are often negligible.)

The classification of neighbors by symmetry, rather than by distance, was needed in some intermediate steps in the calculations of the statistics of large clusters. However, all the *final results* that are actually presented in this series of papers can be expressed using the classification of neighbors by distance, up to the 12th neighbors. This classification is completely equivalent to the classification by symmetry classes, except that it includes only (the most important) twelve symmetry classes. For this reason, in the remainder of this paper, neighbors will be classified as 1st neighbors (NN's), 2nd neighbors, 3rd neighbors, etc., up to the 12th neighbors. The corresponding symmetry classes will be numbered from 1 to 12, as in Fig. 1. Later, these numbers will also be used to label the symmetry classes in some listings.

B. Alternative classifications of the exchange constants

In the present work all exchange interactions are of the Heisenberg type. The interaction between two magnetic ions ("spins"), k and l, has the form

$$\mathcal{H}_{k,l} = -2J(k,l)\mathbf{S}_k \cdot \mathbf{S}_l, \tag{1}$$

where $J(k,l)$ is the exchange constant. Two methods of classifying the various exchange constants (or J's) will be used. The first relates each J to the symmetry class of the relevant neighbor. The second is a classification by relative size.

1. Classification by the neighbor's symmetry class

It is assumed that all the magnetic ions are of one type (e.g., Mn^{2+}). The exchange constant $J(k,l)$ depends on the displacement vector $\mathbf{r}_{kl}$. If the location of spin k is chosen as the "central spin," marked by × in Fig. 1, then spin l, at $\mathbf{r}=\mathbf{r}_{kl}$, is at a neighboring site of a particular symmetry class. Because all neighbors of the same symmetry class have the same $J(k,l)$, any exchange constant can be classified by the neighbor's symmetry class.

The classification of the J's by the neighbors' symmetry classes is appropriate for all cation structures. In our view

this scheme is preferable to the traditional classification of the J's by the neighbors' distances r. The classification by symmetry is especially important when one of the shortest r's corresponds to several symmetry classes, as is the case for NN's in the ideal hcp structure.[11] For the square lattice, however, each of the twelve shortest r's corresponds to only one of the symmetry classes from 1 to 12. Moreover, as a practical matter, it is extremely rare for exchange constants beyond those associated with these twelve symmetry classes to be needed. For these reasons the classification of the J's will be restricted to the following: J_1 for NN, J_2 for 2nd neighbor, and so on up to J_{12}. Later, it will be expedient to restrict the set of J's even further: only the first nine exchange constants, designated by single-digit numbers, from 1 to 9, will be used. Single-digit numbers will result in a significant compression of tables that accompany this series of papers. The nine J's that are included are more than adequate for the vast majority of applications.

2. Classification by size

The classification of the J's by symmetry classes (or distances r, when appropriate) is very useful in theoretical models. However, such a classification can be very impractical in the early stages of an analysis of experimental data. The MST method often yields accurate values for some J's without immediately revealing the corresponding neighbors' symmetry classes.[11] Obviously, until the symmetry class of the relevant neighbor is determined, it cannot be used to classify, or label, the exchange constant. In such a situation it is convenient to classify the J's by their relative size. The largest J is designated as $J^{(1)}$, the second-largest as $J^{(2)}$, etc.

C. Cluster models

As in Ref. 3, the discussion is restricted to a strongly diluted AF material. Let x be the fraction of cation sites that are occupied by magnetic ions (see Ref. 12 for an alternative notation). It is assumed that x is well below the site percolation concentration.[13] The usual theoretical method for treating MST's in this range of x is based on cluster models. The simplest such model is the NN cluster model (or J_1 model), in which only the NN exchange interaction is included. Each cluster then consists of a group of spins, any two of which are connected to each other by at least one continuous path of NN exchange bonds (J_1 bonds). The only exception is an isolated spin, called a "single," with no exchange bonds. Spins in different clusters must not be connected to each other by any continuous path of J_1 bonds.

The J_1–J_2 cluster model includes both J_1 and J_2. Any two spins in the same cluster are then connected by at least one continuous path of J_1 and/or J_2 bonds. Spins in different clusters must not be connected to each other by a continuous path of such bonds. In general, a cluster model includes only a finite subset of all possible J's. The model is designated by the J's that are included. For example, the J_1–J_2–J_5 model includes only exchange interactions (or "bonds") with the 1st, 2nd and 5th neighbors.

D. Cluster Hamiltonian

The only magnetic interactions that are included in this series of papers are (1) isotropic intracluster exchange interactions (Heisenberg exchange) and (2) Zeeman interaction with the magnetic field **B**. The intracluster exchange Hamiltonian is then the sum over all pairs $\langle k,l\rangle$ of the Hamiltonian given by Eq. (1). The g factor in the Zeeman term is assumed to be isotropic. All anisotropies are excluded, and all magnetic ions are assumed to be identical.

E. Cluster types

The assumptions concerning the cluster Hamiltonian lead to the concept of "cluster type." This concept is constructed so that (apart from the numerical values of the g factor and of the J's) all clusters of a given type have the same cluster Hamiltonian. For this reason, cluster types play a central role in the theory of MST's. Cluster types were discussed in Ref. 3. The following more detailed updated discussion is essential for the theory in this series of papers.

All clusters are divided into "types," labeled by the index c. Each cluster type is characterized by (1) the cluster "size," which is the number n_c of spins in the cluster, and (2) the "complete set" of intracluster exchange bonds. This complete set has the following meaning. A cluster with n_c spins contains $n_c(n_c-1)/2$ spin pairs $\langle k,l\rangle$. In reality, any two spins k and l are always coupled to each other by some exchange constant $J(k,l)$. However, any particular cluster model represents an idealization in which only a subset of the $J(k,l)$ are included, and all the other $J(k,l)$ are set equal to zero. The complete set of intracluster exchange bonds specifies: (1) the pairs $\langle k,l\rangle$ for which $J(k,l)$ is not zero in the particular cluster model, and (2) the classification of each of these nonzero $J(k,l)$. The classification is indicated by the single-digit labels, from 1 to 9, introduced in Sec. II B 1. For example, the label 3 means that $J(k,l)=J_3$. The cluster type does not depend on the magnitudes of the nonzero $J(k,l)$. The only relevant fact is that they are nonzero.

F. Bond lists

The exchange Hamiltonian for a cluster may be written as

$$\mathcal{H}_{c,x}=\sum_{k=1}^{n_c-1}\sum_{l=k+1}^{n_c}\mathcal{H}_{k,l}, \tag{2}$$

where $\mathcal{H}_{k,l}$ is given by Eq. (1). The cluster type is specified by a "bond list," which is an ordered list of labels for the exchange constants $J(k,l)$ in this Hamiltonian. The labels can be divided into two groups. (1) Any exchange constant that is not included in the cluster model is labeled by the number "0". (2) Any exchange constant which is included in the cluster model is labeled by the single-digit positive number (from 1 to 9) that identifies its symmetry class.

The ordered list of labels in the bond list matches the sequence of pairs $\langle k,l\rangle$ as it appears in the Hamiltonian of Eq. (2), i.e., it matches the sequence

$$\{\langle 1,2\rangle,\langle 1,3\rangle,\langle 1,4\rangle,\ldots,\langle 1,n_c\rangle;\langle 2,3\rangle,\langle 2,4\rangle,\ldots,\langle 2,n_c\rangle;$$

$$\langle 3,4\rangle,\ldots,\langle 3,n_c\rangle;\quad \ldots;\langle n_c-1,n_c\rangle\}.$$

Because all labels in the bond list are single-digit numbers, the list can be compacted by deleting the commas separating

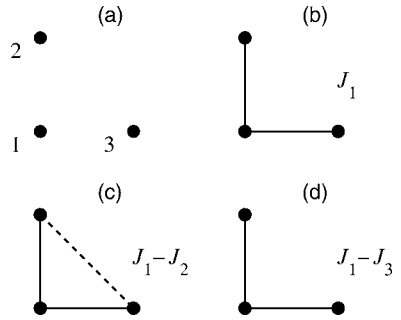

FIG. 2. Exchange bonds for the same triplet in three cluster models: J_1 model, J_1-J_2 model, and J_1-J_3 model. Solid and dashed lines represent J_1 and J_2 bonds, respectively.

the labels. For example, {1,1;0} will be replaced by {11;0}.

The ordered list of labels obtained in this manner depends on the numbering of the spins. To remedy this shortcoming, a numbering scheme which results in a unique ordered list of labels was developed.[14] In this scheme the spins are numbered following an hierarchy based on the exchange bonds attached to each spin. With this numbering scheme, the bond list for each cluster type is unique.

The bond list also gives the cluster size implicitly, because the number of entries in the list is $n_c(n_c-1)/2$. By definition, a single is an isolated spin ($n_c=1$), not connected to any exchange bond. The bond list for a single is therefore empty and will be represented by {}.

As an example, consider a cluster consisting of three spins (i.e., a "triplet"), located in the square lattice as in Fig. 2(a). The first spin is at $(x,y)=(0,0)$, the second at (0, 1) and the third at (1, 0). In the following discussion, it is unnecessary to renumber the spins in this figure.[15]

In the J_1 model there are only two nonzero exchange bonds. They are represented in Fig. 2(b) by the two solid lines. The cluster type in the J_1 model is therefore characterized by a cluster size $n_c=3$, by the pairs $\langle 1,2\rangle$ and $\langle 1,3\rangle$ with nonzero exchange bonds, and by the classification $J(1,2)=J(1,3)=J_1$ of these nonzero exchange constants. The bond list is {11;0}.

Now consider the same three-spin cluster, but in the J_1-J_2 model. There are three nonzero exchange bonds: the two J_1 bonds discussed earlier, represented in Fig. 2(c) by the two solid lines, and one J_2 bond that is represented by a dashed line. The cluster type in the J_1-J_2 model is therefore characterized by the cluster size, $n_c=3$; the pairs $\langle 1,2\rangle$, $\langle 1,3\rangle$, and $\langle 2,3\rangle$ with nonzero exchange bonds; and by the classification of these exchange constants, $J(1,2)=J(1,3)=J_1$ and $J(2,3)=J_2$. The cluster type is different from that in the J_1 model. The bond list in the J_1-J_2 model is {11;2}.

Finally, consider the same three spins again, but in the J_1-J_3 model. The nonzero exchange bonds are shown in Fig. 2(d). They are identical to those in the J_1 model. Therefore, both the cluster type and the bond list are the same as in the J_1 model.

The example just given leads to the following conclusion: the cluster type of the very same cluster may depend on the cluster model. When the cluster model is changed, the cluster type may or may not change. This point will be important in a later paper that treats alternative cluster models. In the present paper, only the NN cluster model is considered. For this model the only labels that appear in the bond lists are 0 and 1.

III. NEAREST-NEIGHBOR CLUSTER MODEL AND ITS STATISTICS

A. Cluster types for the square lattice

1. Organization of the presentation

All cluster types of sizes $n_c \leqslant 12$, for the J_1 model on the square lattice, were identified.[14] There are 3290 such cluster types. To present the results for such a large number of types, the following choices were made.

1. The ten cluster types with sizes $n_c \leqslant 5$ are presented in the paper itself. When the fraction x of magnetic ions is below 0.25, the combined contribution to the magnetization M from these cluster types is the largest contribution by far.

2. The 29 cluster types with sizes $n_c=6$ and 7, and some their properties, are presented in Appendix A.

3. All the 3290 cluster types, for all sizes $1 \leqslant n_c \leqslant 12$, and some of their properties, are presented in the EPAPS attached to the present paper.[16]

2. Cluster types for cluster sizes $n_c \leqslant 5$

The 10 cluster types with sizes $n_c \leqslant 5$ are as follows.

Type $c=1$ is a "single" ($n_1=1$), with an empty bond list { }.

Type $c=2$ is a "pair" ($n_2=2$), with bond list {1}.

Type $c=3$ is a "triplet" ($n_3=3$), with bond list {11;0}. This triplet is a so-called "open" triplet.[3] There are no "closed" triplets for the J_1 model on the square lattice.

There are three types of "quartets" ($n_c=4$), with the following designations and bond lists: 4*A* {110;01;0}; 4*B* {111;00;0}; and 4*C* {011;11;0}. Type 4*A* corresponds to the "string quartet" in Ref. 3, type 4*B* corresponds to the "propeller quartet," and type 4*C* to the "square quartet."

Finally, there are the four types of "quintets" ($n_c=5$): 5*A* {0110;101;00;0}; 5*B* {1011;100;00;0}; 5*C* {0111;110;00;0}; and 5*D* {1111;000;00;0}.

Figure 3 shows the exchange bonds connecting the spins in these 10 cluster types.

B. Configurations

Some cluster types have a unique geometric shape. Examples are the single and the pair in Fig. 3. However, all other cluster types in this figure can have different geometrical shapes. Figure 4 shows some examples. (In Fig. 3, only one geometry is shown for each cluster type, even when that type can have different geometries.) For example, the top part of Fig. 4 shows two possible geometries for cluster type 3 (open triplet). Only one of these appears in Fig. 3.

Different geometries of cluster type c correspond to different "configurations" of that cluster type. Each such configuration is labeled as r_c. A more precise definition of the term "configuration" is the following: two individual clusters belong to the same configuration if and only if one can be

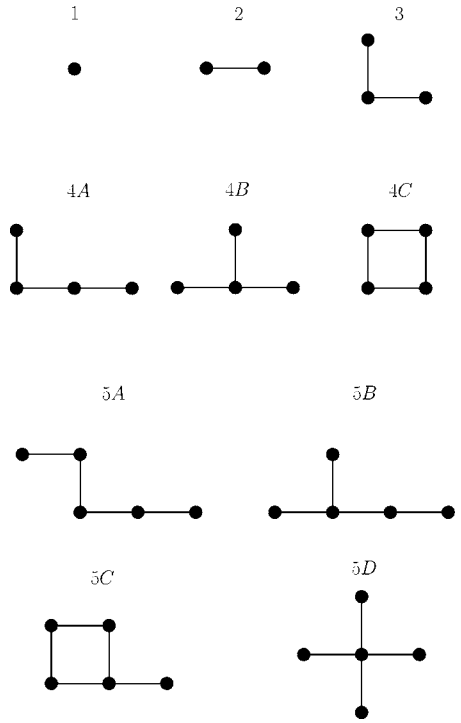

FIG. 3. Exchange bonds (shown as solid lines) connecting the spins (solid circles) in the 10 cluster types with sizes n_c up to 5.

obtained from the other by a symmetry operation of the space group of the cation structure.[3] In the present work these are the operations of the P4*m* space group of the square lattice, including lattice translations. Individual clusters that belong to a configuration are called "realizations" of the configuration.

The above definition of configuration has several implications, regardless of the cation structure. Given a particular realization of a configuration, a geometric object may be constructed by joining all pairs $\langle k,l\rangle$ of cation sites in this realization by straight-line segments. Such an object may also be constructed for any other realization of the same configuration. The definition of a configuration then implies that the two objects are either identical in shape or are chiral isomers of each other. If the objects are identical, they are embedded in the cation structure in the same manner. If they

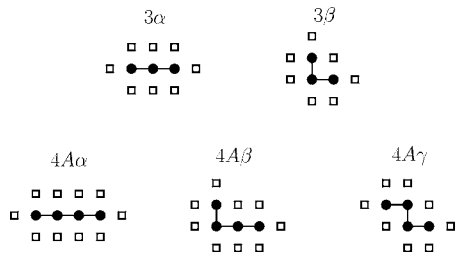

FIG. 4. Upper row: The two configurations 3α (straight), and 3β (L-shaped) of an open triplet (cluster of type 3). Lower row: The configurations $4A\alpha$ (straight), $4A\beta$ (L-shaped), and $4A\gamma$ (zig-zag) of the quartet type 4*A*. The empty squares surrounding each configuration, both in the upper and lower rows, are cation sites that must remain vacant.

are chiral isomers, then both the second object and the cations surrounding it are mirror images of the first object and the cations surrounding it. These properties of realizations of the same configuration have important implications for the statistics of clusters. An early discussion of some of these points was given in the README.TXT file of the EPAPS attached to Ref. 3, and (very briefly) in footnote no. 134 of that reference. Additional discussion is given below.

The upper part of Fig. 4 shows the two configurations of cluster type 3 (open triplet), labeled as 3α and 3β. Cation sites that are occupied by magnetic ions (spins) are shown as solid circles. The empty squares near each of the configurations show surrounding cation sites that are NN's of the occupied sites. These particular surrounding sites must be vacant. Otherwise, the cluster size n_c would exceed 3. The minimum number of sites that must remain vacant is known as the "perimeter," of the configuration,[13,17] and will be labeled as ν_{r_c}. The previously-mentioned geometrical properties of realizations of the same configuration imply that all such realizations have the same perimeter. The perimeter for the 3α configuration in Fig. 4 is $\nu_{3\alpha}=8$. For the 3β configuration, it is $\nu_{3\beta}=7$. The lower row of Fig. 4 shows the three configurations of a string quartet (cluster type 4*A*), labeled as $4A\alpha$, $4A\beta$, and $4A\gamma$. Their perimeters are 10, 9, and 8, respectively.

C. Statistics of cluster types

1. Statistics of cluster types versus statistics of cluster sizes

The end result of the classification of clusters in a diluted material is that each spin belongs to a cluster of a given size, a given type, and a given configuration. As noted earlier, the cluster's Hamiltonian depends only on the cluster type. The relevant statistics is therefore the statistics of cluster types.[18] This statistics differs from the statistics in percolation theory, which is largely the statistics of cluster sizes.[13,17]

The statistics of clusters of type c is constructed from the statistics of the configurations r_c of that cluster type. The procedure is analogous to the one used in the statistics of clusters of a given size. The latter is constructed from the statistics for the configurations of that size.

2. Probability that a spin is in cluster type c

Consider a sample with a mass of 1 kg, in which a fraction x of the cation sites are occupied by magnetic ions (spins).[12] Let the total number of spins in the sample be N_{total}. The "population" N_c of a cluster of type c is defined as the total number of individual clusters (or "realizations") of this cluster type. Similarly, the population N_{r_c} of the configuration r_c is the number of realizations of this configuration. Clearly, N_c is the sum of N_{r_c} over all the configurations r_c.

The probability P_c that is defined below relates not to the population N_c of individual clusters of type c, but to the number of *individual spins* that are in this population. The latter number is $n_c N_c$. This point is noteworthy because many works on percolation theory, e.g., Ref. 13, focus on the number of individual clusters, not on the number of individual spins.

The probability that a randomly chosen spin is in a cluster of type c is

$$P_c = n_c N_c / N_{\text{total}}, \tag{3}$$

and is a function of x. The procedures used to calculate $P_c(x)$ were discussed extensively in the literature,[18] and were outlined in Ref. 3. The crucial assumption is that the magnetic ions are randomly distributed over the cation sites.

The probability P_c is the sum of the probabilities P_{r_c} of finding a randomly chosen spin in each of the configurations r_c of cluster type c. The expression for P_{r_c} is[3]

$$P_{r_c} = n_{r_c} x^{n_c - 1} (1 - x)^{\nu_{r_c}}. \tag{4}$$

The parameter n_{r_c} is the number of different possible realizations of the configuration r_c, subject to the condition that one spin in each realization must be at the origin. The parameter ν_{r_c} is the perimeter of the configuration r_c. For small clusters the task of finding all possible configurations, and the parameters n_{r_c} and ν_{r_c}, is fairly simple. For large clusters, however, it was necessary to use an elaborate computer program.[14] This program was based on the principle that any two realizations of the configuration r_c are related to each other by a symmetry operation of the space group of the square lattice. All realizations of the configuration r_c were generated from one realization (called the "prototype") by the space group operations. The probability P_c was then obtained as the sum of P_{r_c} over all the configurations r_c of cluster type c, i.e.,

$$P_c = \sum_{r_c} n_{r_c} x^{n_c - 1} (1 - x)^{\nu_{r_c}}. \tag{5}$$

A simple (and well known) example is the probability P_3 for the open triplet (cluster of type 3 in Fig. 3). The values of n_{r_c} for the 3α and 3β configurations shown in Fig. 4 are 6 and 12, respectively. Using the perimeters $\nu_{3\alpha}=8$ and $\nu_{3\beta}=7$, one obtains

$$P_{3\alpha} = 6x^2(1 - x)^8 \tag{6a}$$

and

$$P_{3\beta} = 12x^2(1 - x)^7. \tag{6b}$$

The probability P_3 is $P_{3\alpha} + P_{3\beta}$.

Figure 5 shows the probabilities P_1 for singles, P_2 for pairs, and P_3 for triplets as a function of x. Also shown are: the sum P_4 of the probabilities for the three types of quartets, i.e., $P_4 = P_{4A} + P_{4B} + P_{4C}$; the sum P_5 of the probabilities for the four types of quintets; the probability $P_{>5}$ that a spin is in a cluster with size $n_c > 5$; and the probability $P_{>12}$ that a spin is in a cluster with $n_c > 12$. The range of x, up to 0.5, is below the site percolation concentration $x = 0.593$ for the J_1 model on the square lattice.[13] The probabilities for each of the quartet and quintet types are shown individually in Fig. 6.

Several features of Figs. 5 and 6 are noteworthy.

(1) In the range $x < 0.25$ (at least) the probability P_1, for singles, is the largest among all P_c's.

(2) Among cluster types with sizes $n_c > 1$, the probability P_2 for pairs is the largest.

(3) The probability P_3 for the only existing triplet type is larger than the probability sums P_4 or P_5. Therefore, P_3 is larger than P_c for any one type of quartet or any one type of quintet.

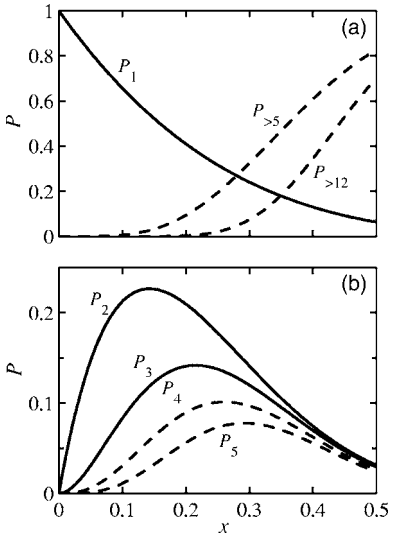

FIG. 5. Various probabilities P for the J_1 model on the square lattice, plotted as a function of the fraction x of cations that are magnetic. Solid curves are probabilities P_c for individual cluster types. Dashed curves are sums of probabilities P_c. Some of these sums are over all cluster types of a given size. Others are sums over all cluster types with sizes larger than a specified size. Part (a) shows the probability P_1 for singles, and the sums $P_{>5}$ and $P_{>12}$ for sizes exceeding 5 and 12, respectively. Part (b) shows the probabilities P_2 and P_3 for pairs and triplets, respectively, and the sums P_4 and P_5 over all quartet types and over all quintet types, respectively.

These trends are even more pronounced for the populations N_c, which count individual clusters instead of individual spins. From Eq. (3), the ratio between the populations

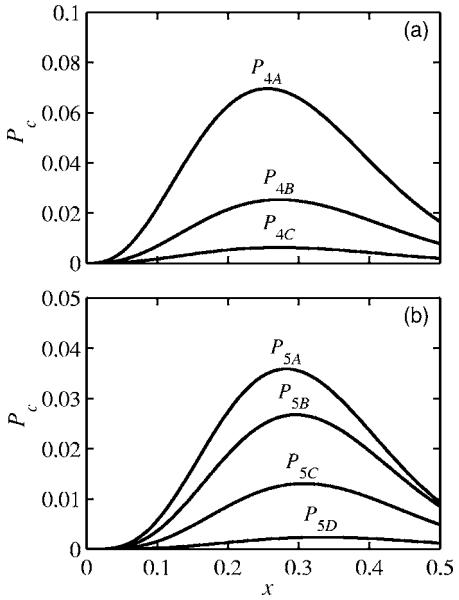

FIG. 6. (a) Probabilities P_c for the three types of quartets: 4*A*, 4*B*, and 4*C*. (b) Probabilities P_c for the four types of quintets: 5*A*, 5*B*, 5*C*, and 5*D*.

of pairs and triplets is $N_2/N_3=(3/2)P_2/P_3$. The ratio between the populations of pairs and string quartets (type $4A$) is $N_2/N_{4A}=2P_2/P_{4A}$, etc. For low x the pair population N_2 is by far the largest among the populations of cluster types that produce MST's. The MST's from pairs then have the largest magnitude by far, and are the most suitable for determining J_1.

3. Perimeter polynomials for cluster types

Perimeter polynomials (PP's) are used to express results of cluster statistics succinctly. Typically, they are used to compress expressions for the number of individual clusters of size s ("population" for size s, in our terminology), normalized to the total number of sites that can be occupied by spins.[13,17] Here, the concept of PP is adapted for compressing the results for the probabilities P_c for cluster *types*. For the 10 cluster types in Fig. 3, PP's are merely a convenience. However, for the more than 3000 other cluster types, the compression achieved with the PP's is almost a necessity.[19]

The starting point for defining the PP for cluster type c is Eq. (5). The first, and most important, step is to group together all terms that have the same perimeter v_{r_c}. Next, the symbol for the probability that a cation site is vacant is changed from $(1-x)$ to q,

$$q \equiv (1-x). \tag{7}$$

This change is made in order to conform with the usual notation used for PP's.[12] Finally, the cluster size n_c is factored out. The last step bridges between the census of individual spins and the census of individual clusters [see Eq. (3)]. With these changes, Eq. (5) takes the form

$$P_c = n_c x^{n_c-1} D_c(q), \tag{8}$$

where $D_c(q)$ is a polynomial in q. This polynomial is defined as the PP for cluster *type* c. The conventional perimeter polynomial $D_s(q)$ for cluster *size* s is the sum of $D_c(q)$ over all cluster types c of size $n_c=s$, i.e.,

$$D_s(q) = \sum_{c,n_c=s} D_c(q). \tag{9}$$

Table I gives the PP's $D_c(q)$ for the ten cluster types with sizes $n_c \leqslant 5$. These are the cluster types shown in Fig. 3. The PP's for the 29 cluster types with sizes $n_c=6$, 7 are given in Appendix A. The PP's for all cluster types with $8 \leqslant n_c \leqslant 12$ are given in the EPAPS that accompany this paper.[16]

Two checks of the present results for $D_c(q)$ were made. First, for the NN cluster model on the square lattice, the conventional PP's for cluster *size*, $D_s(q)$, were given decades ago by Sykes and Glen.[17] Comparison between their results and the $D_c(q)$ given here confirms that Eq. (9) is satisfied. Second, the PP's for cluster types with $n_c \leqslant 4$ can be obtained easily from Fig. 8 of Ref. 13. The results agree with those in Table I.

TABLE I. Perimeter polynomials $D_c(q)$ for the 10 cluster types with sizes $n_c \leqslant 5$. The notation for the cluster types follows Fig. 3.

n_c	Type c	$D_c(q)$
1	1	q^4
2	2	$2q^6$
3	3	$4q^7+2q^8$
4	$4A$	$4q^8+8q^9+2q^{10}$
	$4B$	$4q^8$
	$4C$	q^8
5	$5A$	$4q^9+16q^{10}+12q^{11}+2q^{12}$
	$5B$	$8q^9+12q^{10}$
	$5C$	$8q^9$
	$5D$	q^8

IV. EQUILIBRIUM MAGNETIZATION CURVE

A. Average magnetic moment of a realization of one cluster type

Consider a sample in thermal equilibrium at a temperature T and magnetic field B. A key assumption of all cluster models is that in calculations of thermodynamic equilibrium properties, individual clusters may be considered as independent of each other.[20] The procedure for calculating the average magnetic moment $\mu_c(T,B)$ of an individual cluster of type c (realization of cluster type c) was outlined in Ref. 3. The cluster Hamiltonian is diagonalized at $B=0$, and the energy eigenvalues are used to calculate $\mu_c(T,B)$ using Eq. (23) of that reference. Unlike P_c, both the energy eigenvalues and $\mu_c(T,B)$ depend on the spin S of the individual magnetic ions. Because the experimental work in the following paper involved the Mn^{2+} ion, theoretical results for $S=5/2$ will receive greater attention in the discussion below.

Figure 7 shows the results for μ_c at $T=0$ for all cluster types with $n_c \leqslant 5$. They are plotted as a function of the reduced magnetic field

$$b = g\mu_B B/|J_1|, \tag{10}$$

where μ_B is the Bohr magneton. These results are for $S=5/2$. All cluster types, except the "single," exhibit MST's. The values of b at the MST's were given earlier.[21] For completeness they are repeated in Table II. For the purpose of determining the exchange constant J_1, the most important MST's are from pairs. For $S=5/2$ these MST's occur at $b=2$, 4, 6, 8, and 10. For an arbitrary S the MST's from pairs occur at

$$g\mu_B B_n = 2|J_1|n, \tag{11}$$

where $n=1,2,\ldots,2S$.

At $T=0$, some cluster types in Fig. 7 exhibit an abrupt rise at $b=0$. This abrupt rise occurs for singles, triplets, quartets of type $4B$, and quintets of all types. These cluster types are those for which the total spin S_T of the ground state at $b=0$ is not zero. The ground-state total spin at $b=0$, for a realization of cluster type c, is defined as the spontaneous total spin $S_c(0)$. Any cluster type, of whatever size, for which $S_c(0)$ is

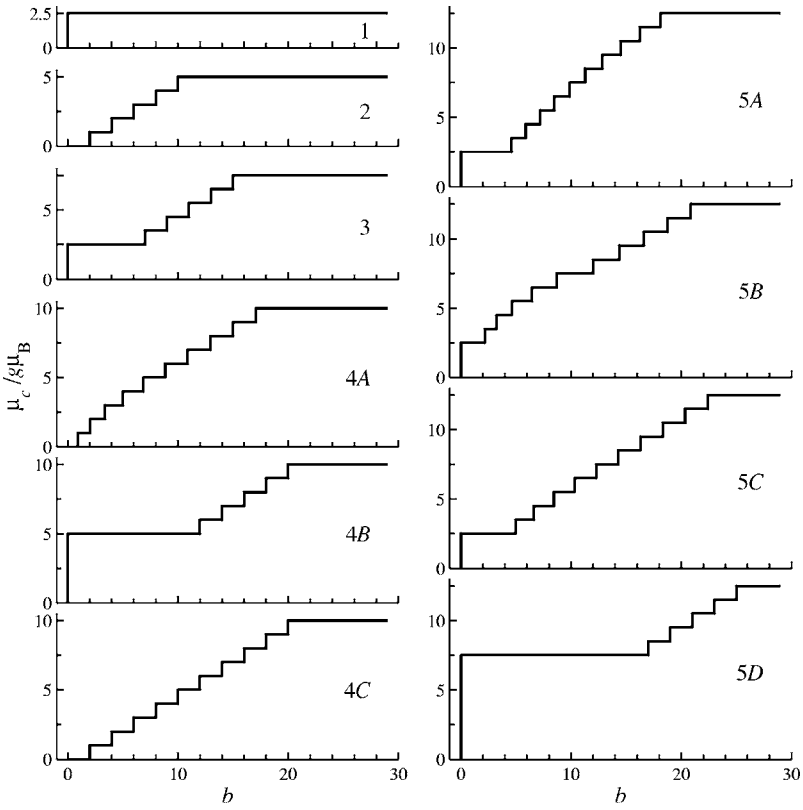

FIG. 7. Average zero-temperature magnetic moment μ_c for all cluster types of size $n_c \leqslant 5$, plotted as a function of reduced magnetic field $b=g\mu_B B/|J_1|$. These results are for $S=5/2$. The notation for the cluster types is as in Fig. 3. Note the position of the zero on the abscissa scale.

not zero, exhibits a rapid rise of μ_c at low fields. The rapid rise represents the alignment of $S_c(0)$ by the magnetic field. Its field dependence follows the Brillouin function (BF) for spin $S_c(0)$.

When $b \to \infty$, both the magnitude S_T of the total spin and its component S_{Tz} along **B**, reach the saturation value $S_c(\infty) = n_c S$. The ratio between the magnitude of the low-field rapid rise of μ_c and the saturation value of μ_c is, therefore,

$$\eta_c = S_c(0)/n_c S. \tag{12}$$

Values of η_c for clusters types c with sizes $n_c \leqslant 5$ are listed in Table II. Values of η_c for cluster types with $n_c=6, 7$ are given in Appendix A, and those for cluster types with $8 \leqslant n_c \leqslant 12$ are given in the EPAPS.[16] For the NN cluster model on the square lattice, η_c is independent of S. The reason is that there is no frustration in this case. For other lattices and/or other cluster models, η_c may depend on S (see Appendix B for the calculation of η_c).

TABLE II. Values of $\eta_c = S_c(0)/n_c S$, and of the reduced fields b_n at the MST's, for clusters types with sizes $n_c \leqslant 5$. The values of b_n are for $S=5/2$, but those for η_c are for any S.

Type	η_c	b_n				
2	0	2	4	6	8	10
3	1/3	7	9	11	13	15
4*A*	0	0.950	2.041	3.389	5.023	6.873
		8.849	10.883	12.941	15.006	17.071
4*B*	1/2	12	14	16	18	20
4*C*	0	2	4	6	8	10
		12	14	16	18	20
5*A*	1/5	4.617	5.889	7.177	8.494	9.858
		11.293	12.829	14.482	16.245	18.090
5*B*	1/5	2.166	3.206	4.630	6.458	8.700
		11.995	14.384	16.600	18.744	20.850
5*C*	1/5	4.946	6.629	8.428	10.315	12.268
		14.265	16.288	18.324	20.364	22.406
5*D*	3/5	17	19	21	23	25

B. Expression for the total magnetization

The equilibrium magnetization $M(T,B)$ is obtained by summing the contributions from all cluster types, taking their populations into account. That is,

$$M(T,B) = \sum_c N_c \mu_c(T,B) = N_{\text{total}} \sum_c \frac{P_c}{n_c} \mu_c(T,B). \tag{13}$$

In practice this infinite sum cannot be carried out, because only cluster types for which both N_c and μ_c have been obtained previously can be included. The infinite sum is therefore truncated after carrying out the finite sum over cluster types with known N_c and μ_c. Typically, this finite sum includes clusters up to a maximum size, $n_c = n_{\max}$. The remainder, after the truncation, is replaced by a "remainder correction" $R(T,B)$.

The function $R(T,B)$ should approximate the true remainder at all fields. In addition, after $R(T,B)$ is included, the calculated M in the limit $b \to \infty$ is required to reproduce the *exact* saturation value of M. The saturation value M_0, per kg, is

$$M_0 = N_{\text{total}} g \mu_B S. \tag{14}$$

The procedure of treating clusters with $n_c \leqslant n_{\max}$ exactly, but the larger clusters in the remainder only approximately, is appropriate only if the percentage of spins in the remainder is small. The percentages of spins with sizes larger than 5, or larger than 12, are given by the curves $P_{>5}$ and $P_{>12}$ in Fig. 5, respectively. To keep this percentage low, the range of x must be restricted. Examples of magnetization curves calculated with $n_{\max}=5$ for the range $x \leqslant 0.20$ will be shown later. All these examples are for $S=5/2$. The value $n_{\max}=5$ was dictated by the maximum cluster size for which the energy eigenvalues were obtained. The maximum size, $n_c=12$, for the results of the cluster statistics was not the limiting factor.

C. Remainder corrections

For $n_{\max}=5$, the percentage of spins that are in the remainder increases from 0.6% at $x=0.10$, to 3.3% at $x=0.15$, and to 9.4% at $x=0.20$ (see the plot for $P_{>5}$ in Fig. 5). For many purposes even a rough approximation of the remainder is adequate for $x \leqslant 0.2$. Ignoring the remainder altogether, instead of approximating it, is a much poorer alternative.

Two methods of approximating the remainder were used: (1) the "rise-and-ramp" (R&R) approximation and (2) the corrective clusters (CC) method. Early versions of these methods were mentioned in Ref. 3. The R&R approximation is specific to the J_1 model. The CC method can be generalized to other models, as will be illustrated in a later paper.

1. The rise and ramp approximation

In the R&R approximation the function $R(T,B)$ is a sum of two terms: a fast rise at low B, and a "ramp." Thus,

$$R(T,B) = M_{\text{rise}} + M_{\text{ramp}}. \tag{15}$$

The term M_{rise} is due to the rapid alignment of $S_c(0)$, for those clusters in the remainder that have nonzero $S_c(0)$. The saturation value of M_{rise} may be written as

$$(M_{\text{rise}})_{\max} = \eta_{>5} P_{>5} M_0, \tag{16}$$

where $\eta_{>5}$ is a numerical constant representing the average value per spin of the parameter η_c for the clusters in the remainder. It is given by

$$\eta_{>5} = \frac{\sum_{c,n_c>5} \eta_c P_c}{\sum_{c,n_c>5} P_c} \tag{17a}$$

or

$$\eta_{>5} = \frac{1}{P_{>5}} \sum_{c,n_c>5} \eta_c P_c. \tag{17b}$$

The sums in Eqs. (17a) and (17b) are over all clusters types c with sizes $n_c>5$. A similar notation will be used for other sums over all cluster types c that satisfy a restriction on the cluster size n_c.

The so-called ramp in Eq. (15) actually consists of a true linear ramp up to a certain effective saturation field B_s, followed by a constant at higher fields. The linear ramp approximates the superposition of the "staircases" of MST's from the clusters in the remainder. It is given by

$$M_{\text{ramp}} = (1-\eta_{>5}) P_{>5} M_0 \frac{B}{B_s} \quad \text{for } B \leqslant B_s. \tag{18a}$$

For fields above B_s the term M_{ramp} in Eq. (15) is given by the constant

$$M_{\text{ramp}} = (1-\eta_{>5}) P_{>5} M_0 \quad \text{for } B > B_s. \tag{18b}$$

With this constant value the calculated magnetization, after the remainder correction, reproduces the exact saturation value M_0. The reduced field corresponding to B_s is b_s.

In an early version of the R&R approximation for a $3D$ material,[21] the parameters $\eta_{>5}$ and b_s were treated as constants, independent of x. The values that were chosen for $S=5/2$ were $\eta_{>5}=1/7$, and $b_s=21$. The magnetic-field dependence of M_{rise} was assumed to follow the BF for spin $S=5/2$, i.e., $\mathcal{B}_{5/2}(\xi)$, where

$$\xi = \frac{g\mu_B SB}{k_B T}. \tag{19}$$

More recently, an improved x-dependent version of the R&R approximation was given for the diluted Heisenberg chain.[8]

The version that is used in the present work takes advantage of new results for cluster types c with sizes $6 \leqslant n_c \leqslant 12$. These new results [for P_c, η_c, and the reduced saturation field $b_s(c)$], are reported in Appendix A and in the EPAPS that accompany the present paper.[16] The fast rise at low B is given by

$$M_{\text{rise}} = M_0 \sum_{c,n_c>5} \eta_c P_c \mathcal{B}_c(\xi_c), \tag{20}$$

where $\mathcal{B}_c(\xi_c)$ is the BF for spin $S_c(0)$. The parameter ξ_c is given by Eq. (19) for spin $S=S_c(0)$.

The sums in Eqs. (17a), (17b), and (20) are examples of functions of the form

$$f = \sum_{c,n_c>5} F_c P_c \tag{21}$$

that appear in connection with the remainder. The only known terms in these infinite sums are those for cluster types with $n_c \leqslant 12$. The other terms, from larger clusters, represent only a fraction of the small percentage of spins that are in the remainder. This fraction, $P_{>12}/P_{>5}$, increases with x, and it reaches the value 10.9% at $x=0.25$. These 10.9% of the spins in the remainder correspond to 2.1% of the total number of spins.

In the range of $x \leqslant 0.25$, sums having the form of Eq. (21) will be approximated by assuming that spins in clusters of sizes $n_c>12$ have the average properties of spins in clusters of sizes $n_c=11,12$. That is,

$$f \approx \sum_{c,6\leqslant n_c\leqslant 12} F_c P_c + \frac{P_{>12}}{P_{11}+P_{12}} \sum_{c,n_c=11,12} F_c P_c, \tag{22}$$

where P_{11} and P_{12} are the sums of the probabilities P_c over all cluster types of sizes 11 and 12, respectively. The reason

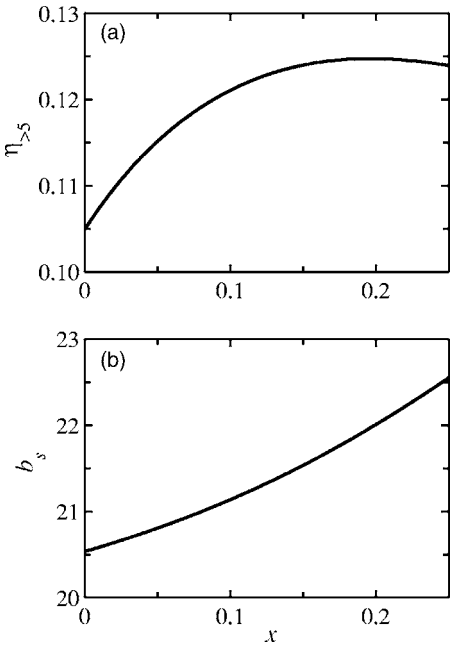

FIG. 8. x dependence of the parameters $\eta_{>5}$ and b_s in Eq. (23) for the linear ramp. (a) $\eta_{>5}$, for any value of S; (b) b_s for $S=5/2$.

for using both sizes 11 and 12 in the last term of Eq. (22) is that some of the functions F_c depend somewhat on whether n_c is even or odd. Equation (22) was used to approximate the infinite sums in Eqs. (17b) and (20).

Using the reduced magnetization $m=M/M_0$ and the reduced magnetic field b, Eq. (18a) for the linear ramp may be expressed as

$$m_{\text{ramp}} = (1-\eta_{>5})P_{>5}(b/b_s) \quad \text{for } b \leqslant b_s. \tag{23}$$

The value of $1/b_s$ is a weighted average of the inverse reduced saturation fields $1/b_s(c)$ for the cluster types that are in the remainder. The weight for each cluster type c is proportional to its maximum contribution to the linear ramp. The x-dependent value of $1/b_s$ is given by

$$\frac{1}{b_s} = \frac{\sum_{c,n_c>5}(1-\eta_c)P_c/b_s(c)}{\sum_{c,n_c>5}(1-\eta_c)P_c}. \tag{24}$$

The results for $\eta_{>5}$ and b_s are shown in Fig. 8. The sums in Eqs. (17b) and (24) were evaluated using the approximation given by Eq. (22). The results for b_s are for $S=5/2$. Values of b_s for other S can be obtained by noting that b_s is proportional to S (see Appendix C).

The use of a single linear ramp to represent the superposition of the staircases from all cluster types in the remainder is, of course, a drastic simplification. The staircases in Fig. 7 are for smaller clusters than those in the remainder. Nevertheless, they are suggestive of the expected behavior of the clusters in the remainder. For some cluster types, such as 3 and 5D, the staircases in Fig. 7 start at a value of b which is substantially larger than 1. Those staircases in the true remainder that behave in this manner make no contribution to the linear ramp at low b. If all staircases of the true remainder behaved in this manner, a linear ramp would have overestimated their contribution at low b. However, for other staircases in Fig. 7 (e.g., cluster type 4A) the stairs are more closely spaced at low b than at higher b. If all staircases in the true remainder behaved in that manner, a single linear ramp would have underestimated the remainder at low b. The use of a single linear ramp is a compromise.

The results of the R&R approximation are compared later with the results of the corrective quintets (CQUIN's) method. For $x<0.15$, less than 3% of the spins are in the remainder. For this range of x we expect the accuracy of the R&R approximation to be better than a fraction of 1% of the total value of M. For $x=0.20$, with 9.4% of the spins in the remainder, the expected accuracy is better than about 1%.

2. The corrective clusters method

In the corrective clusters (CC) method the remainder of Eq. (13) is replaced by the magnetization of an "appropriate mixture" of fictitious clusters of size $n_{\max}$. The so-called "corrective quartets" method mentioned in Ref. 3 was for $n_{\max}=4$. In the present paper, $n_{\max}=5$, so that the remainder is replaced by a mixture of fictitious "corrective quintets" (CQUIN's). The CC method may then be called the CQUIN's method.

The CQUIN's method can be expressed succinctly by the following expression for the remainder $R(T,H)$ of the last sum in Eq. (13),

$$R(T,H) = \frac{P_{>5}}{P_5} N_{\text{total}} \sum_{c,n_c=5} \frac{P_c}{n_c} \mu_c(T,B), \tag{25}$$

where $P_{>5}$ and P_5 are defined in Sec. III C 2. This equation has the following physical meaning. The cluster types c of the CQUIN's are the same as the cluster types of the true quintets. The ratios between the populations of the various types of CQUIN's are chosen to be equal to the corresponding population ratios for the true quintets. The total number of spins in all the CQUIN's is the same as the total number of spins in the true remainder. The last condition forces the calculated magnetization to reach the true saturation value M_0 at high fields.

The CQUIN's method artificially increases the size of the magnetization jumps at the MST's from the quintets. As a result, the peaks in dM/dH at the MST's from the quintets are larger than they should be. These artificial effects are large when $P_{>5}$ is larger than P_5. The true peaks in dM/dH at the MST's from the quintets can be obtained by differentiating the magnetization curve obtained without the CQUIN's. Of course, the overall agreement between the calculated and true magnetization curves is improved substantially by including the CQUIN's.

D. Examples of calculated magnetization curves

1. Zero-temperature results for x=0.10

Figure 9(a) shows the calculated magnetization curve for $x=0.10$ at $T=0$, assuming $S=5/2$. The plot is of the reduced magnetization m as a function of the reduced magnetic field

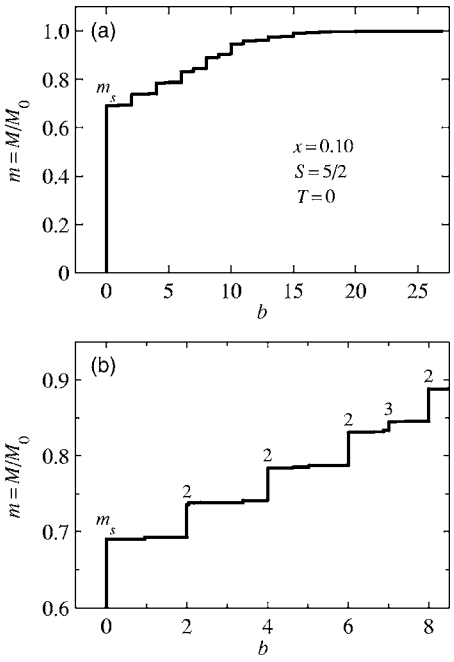

FIG. 9. Calculated reduced magnetization $m=M/M_0$ as a function of the reduced magnetic field $b=g\mu_B B/|J_1|$. These results are for $x=0.10$ at $T=0$, assuming $S=5/2$. (a) Results for reduced fields up to magnetic saturation. (b) Expanded view of the results for $b<8.5$. The MST's labeled as 2 and 3 are from pairs and triplets, respectively. The plateau corresponding to the apparent saturation of the magnetization is labeled as m_s.

b. The remainder, which contains only 0.63% of the spins, was included using the R&R approximation. The expected accuracy for M is about 0.1%. Figure 9(b) gives an expanded view of the magnetization curve for the range $b<8.5$. The largest MST's, labeled as 2, are almost entirely due to pairs. The MST labeled as 3 is the first MST from triplets. The MST's from quartets of type $4A$, the first of which is at $b=0.95$, are barely visible.

Figures 9(a) and 9(b) also show a large jump in the magnetization at $b=0$. This jump is due to the alignment of $S_c(0)$ in all cluster types with $S_c(0)>0$. The jump ends in a plateau at which the reduced magnetization is m_s. The magnetization $M_s=m_s M_0$ at this plateau is known as the "apparent saturation value" (also "technical saturation value").[3] The plateau ends when the first MST of non-negligible size appears.[22] In some experiments the highest available magnetic field may be insufficient for reaching the first MST of non-negligible size. The plateau would then give the false impression that the magnetization has saturated.

2. Results for x=0.20

The zero-temperature magnetization curve for $x=0.20$ is shown in Fig. 10(a). The R&R approximation was used for the remainder (9.4% of the spins in this case). The remainder obtained with this approximation is represented by the solid curve at the bottom of the figure. Also shown at the bottom is the remainder as approximated by the CQUIN's method (dashed line). The two approximations of the remainder differ by less than about 1% of the total magnetization.

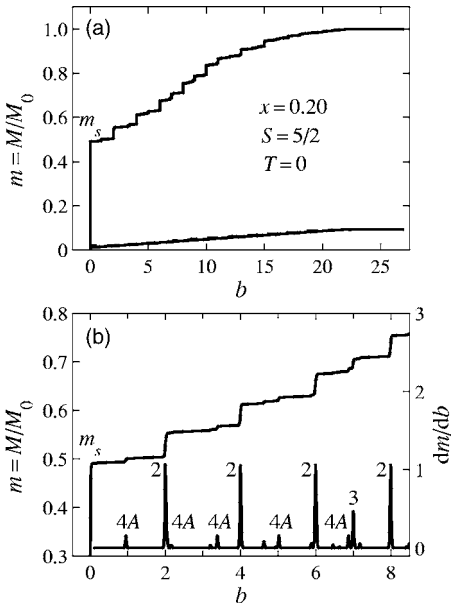

FIG. 10. (a) Calculated reduced magnetization m at $T=0$ for $x=0.20$ and $S=5/2$. The R&R approximation was used for the remainder. The solid and dashed curves at the bottom of the figure represent the remainder corrections obtained from the R&R approximation and from the CQUIN's method, respectively. (b) The upper curve shows an expanded view of the low-field results in part (a). The plateau corresponding to the apparent saturation is labeled as m_s. The lower curve is the normalized susceptibility dm/db, computed at $k_B T/|J|=0.01$ to avoid the infinities at $T=0$. The cluster types making the dominant contributions to the most conspicuous susceptibility peaks are indicated. Peaks labeled as 2 (i.e., from pairs) also contain small contributions from quartets of type $4C$. Small peaks that are visible but are not labeled are from various types of quintets.

Figure 10(b) gives an expanded view of the results in low fields, $b<8.5$. In addition to the MST's from pairs, which are the largest, the first MST from triplets, and MST's from some quartet and quintet types, are also visible. Each of the MST's attributed to pairs (labeled as 2) also contains a small contribution from quartets of type $4C$ (see Table II). Comparison with Fig. 9(b) indicates that the value of m_s (the reduced apparent saturation value) for $x=0.2$ is smaller than for $x=0.1$.

Figure 11 is for the same parameters as Fig. 10(b), except that the normalized temperature $k_B T/|J_1|$ is 0.1 instead of zero. The finite temperature broadens both the fast magnetization rise that starts at $b=0$, and all the MST's. Some of the smaller MST's are then less obvious than at $T=0$. The plateau corresponding to the apparent saturation still stands out clearly.

E. Apparent saturation value

The apparent saturation value of the magnetization is M_s. The corresponding reduced value m_s is given by

$$m_s \equiv M_s/M_0 = \sum_c \eta_c P_c, \tag{26}$$

where the sum is on all cluster types c. The sum over cluster types with sizes $n_c \leqslant 12$ was carried out exactly, and the re-

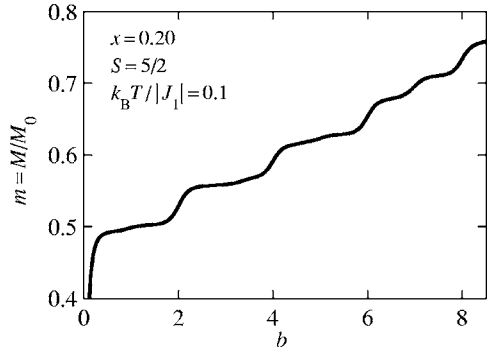

FIG. 11. The magnetization curve for $x=0.20$ for the same parameters as in Fig. 10(b), except that the normalized temperature is $k_BT/|J_1|=0.1$, instead of zero.

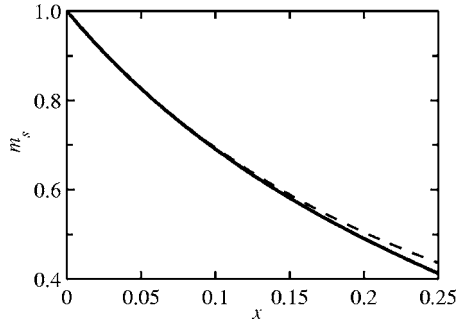

FIG. 12. The reduced apparent saturation value of the magnetization, $m_s=M_s/M_0$, as a function of x, up to $x=0.25$. The solid curve is based on the present work. The dashed curve is based on an earlier, less accurate, treatment (see text).

mainder was approximated by a method analogous to that given by Eq. (22). The results for $m_s=M_s/M_0$ in the range $x\leqslant 0.25$, are represented by the solid curve in Fig. 12. Near the top of this range of x, the expected accuracy is better than a fraction of 1%. At lower x, the expected accuracy is higher. The plot in Fig. 12 is independent of S. The reason is that in Eq. (26), P_c is always independent of S, and η_c is also independent of S for the NN cluster model on the square lattice (see Appendix B).

In early treatments of m_s, only the contributions of clusters with sizes $n_c\leqslant 3$ were treated exactly. The contribution from larger clusters was approximated by setting $\eta_{>3}$ (the weighted average of η_c for $n_c>3$) equal to 0.20, at all values of x.[2,3] This early approximation is represented by the dashed curve in Fig. 12. Overall, the difference between the solid and dashed curves in Fig. 12 is small, but it increases with x. At $x=0.25$ the difference reaches $0.06m_s$, which is an order of magnitude larger than the uncertainty in the solid curve.

ACKNOWLEDGMENTS

This work was supported by CNPQ and FAPESP. Travel funds for Y.S. were also provided by FAPESP.

APPENDIX A: CLUSTER TYPES OF SIZES $n_c=6,7$, FOR THE NN CLUSTER MODEL ON THE SQUARE LATTICE

Various properties of all cluster types c of size $n_c=6$ are given in Fig. 13. For each cluster type, the figure shows the bond list, an example (one configuration), the perimeter polynomial $D_c(q)$, the reduced magnetic field $b_s(c)$ at the last MST for $S=5/2$, and the parameter η_c. Figure 14 gives similar information for all cluster types of size $n_c=7$.

APPENDIX B: COMPUTATION OF η_c

The square lattice can be divided in two interpenetrating sublattices, A and B. In the J_1 model, any spin in sublattice A

Type c	Bond List	Example	$D_c(q)$	$b_s(c)$	η_c
$6A$	{01010;0101;100;00;0}		$4q^{10}+24q^{11}+36q^{12}+16q^{13}+2q^{14}$	18.6603	0
$6B$	{10011;1000;100;00;0}		$8q^{10}+32q^{11}+12q^{12}$	21.0716	1/3
$6C$	{11100;0010;001;00;0}		$4q^{10}+16q^{11}+12q^{12}$	21.5139	0
$6D$	{11100;0011;000;00;0}		$4q^{10}$	22.8078	0
$6E$	{10110;0001;110;00;0}		$8q^{10}+8q^{11}$	22.8078	0
$6F$	{01110;1101;000;00;0}		$8q^{10}$	23.6603	1/3
$6G$	{11010;0101;100;00;0}		$12q^{10}$	24.0680	0
$6H$	{11100;0011;010;01;0}		$2q^{10}$	25.0000	0
$6I$	{10111;1000;000;00;0}		$4q^{10}$	25.4307	1/3
$6J$	{01111;1100;000;00;0}		$4q^{9}$	26.1803	1/3

FIG. 13. Various properties of cluster types c of size $n_c=6$: the bond list; an example (one configuration); the perimeter polynomial $D_c(q)$; the reduced field $b_s(c)$ at the last MST for $S=5/2$; and the value of $\eta_c=S_c(0)/n_cS$.

Type c	Bond List	Example	$D_c(q)$	$b_s(c)$	η_c
$7A$	{010010;01001;0100;100;00;0}	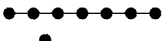	$4q^{11}+36q^{12}+76q^{13}+60q^{14}+20q^{15}+2q^{16}$	19.0097	1/7
$7B$	{100011;10000;1000;100;00;0}		$8q^{11}+48q^{12}+56q^{13}+12q^{14}$	21.1416	1/7
$7C$	{011100;10010;0000;001;00;0}		$8q^{11}+56q^{12}+80q^{13}+24q^{14}$	21.6710	1/7
$7D$	{111000;00100;0010;001;00;0}	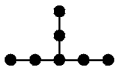	$4q^{12}+8q^{13}+4q^{14}$	22.0711	1/7
$7E$	{011100;10011;0000;000;00;0}	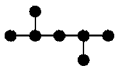	$4q^{11}+18q^{12}$	22.0711	3/7
$7F$	{001110;01001;0110;000;00;0}	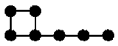	$8q^{11}+24q^{12}+8q^{13}$	22.8861	1/7
$7G$	{110100;00011;1000;000;00;0}	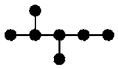	$8q^{11}+16q^{12}$	23.1433	1/7
$7H$	{100011;01100;1100;000;00;0}		$8q^{11}$	23.8786	1/7
$7I$	{001110;11100;0001;000;00;0}		$16q^{11}+16q^{12}$	23.8786	1/7
$7J$	{110010;01100;0100;001;00;0}	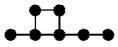	$24q^{11}+24q^{12}$	24.3040	1/7
$7K$	{110100;01010;1001;000;00;0}		$16q^{11}$	25.1516	1/7
$7L$	{100111;10000;1000;000;00;0}	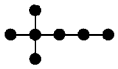	$8q^{11}+4q^{12}$	25.4825	3/7
$7M$	{110011;01000;0100;000;00;0}	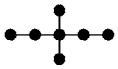	$6q^{12}$	25.8212	1/7
$7N$	{101001;10100;1010;000;10;0}		$16q^{11}$	25.8212	1/7
$7O$	{101110;00001;1100;000;00;0}		$8q^{11}$	26.5032	1/7
$7P$	{011011;11100;0000;000;00;0}		$8q^{10}$	26.5682	3/7
$7Q$	{110011;01100;1000;000;00;0}		$8q^{10}$	27.0711	1/7
$7R$	{001111;01100;0011;000;00;0}		$2q^{10}$	27.0711	1/7
$7S$	{111001;00110;0100;010;00;0}		$4q^{10}$	27.7250	1/7

FIG. 14. Various properties of cluster types c of size $n_c=7$: the bond list; an example (one configuration); the perimeter polynomial $D_c(q)$; the reduced field $b_s(c)$ at the last MST for $S=5/2$; and the value of $\eta_c=S_c(0)/n_cS$.

interacts only with spins in sublattice B. If J_1 is AF then in the ground state at zero magnetic field the spins on each sublattice are parallel to each other, and spins on sublattice A are antiparallel to those on sublattice B. Every AF bond is then fully satisfied (no frustration). Any cluster of size n_c then has n_A spins on sublattice A, and $n_B=n_c-n_A$ spins on sublattice B. Its zero-field ground state has a total spin $S_c(0)=|n_A-n_B|S$, which leads to $\eta_c=|n_A-n_B|/n_c$, independent of S.

As an example, consider cluster type $7L$ in Fig. 14 of Appendix A. There are 5 spins on one sublattice, and 2 on the other. The value of η_c is therefore $3/7$.

The calculation of η_c may be more involved for cluster models other than the J_1 model, and for lattices other than a square. For instance, unlike the square lattice, some lattices (e.g., fcc) allow closed J_1 triplets to exist. For such a closed triplet, $S_c(0)=0$ if S is an integer, in which case $\eta_c=0$. However, if S is an odd half-integer then $S_c(0)=1/2$, so that $\eta_c=1/6S$, which depends on S.

APPENDIX C: CALCULATION OF THE MAGNETIC FIELD AT THE LAST MST

This appendix describes the calculation of the reduced magnetic field $b_s(c)$ at the last MST for cluster type c. This is

also the reduced saturation field for cluster type c at $T=0$. The calculation method is restricted to the NN cluster model, but is valid for any cation lattice structure, regardless of its dimensionality.

For the J_1 model with an AF exchange ($J_1<0$), Eq. (2) for the exchange Hamiltonian for a cluster of type c may be rewritten as

$$\mathcal{H}_{c,x}=\frac{1}{2}|J_1|\sum_k\sum_l j_{kl}2\mathbf{S}^k\cdot\mathbf{S}^l, \tag{C1}$$

where j_{kl} is 1 if the spins k and l are NN's, but is 0 otherwise. These values for j_{kl} happen to coincide with the labels for $J(k,l)=J(l,k)$ in this cluster model, and they can therefore be obtained from the bond list. The matrix $\boldsymbol{j}$, composed of the elements j_{kl}, is symmetric and all its diagonal elements are equal to 0. The total cluster Hamiltonian is

$$\mathcal{H}_c=\mathcal{H}_{c,x}-g\mu_B B\sum_{k=1}^{n_c}S_z^k. \tag{C2}$$

The cluster Hamiltonian commutes with both the magnitude S_T of the total spin of the cluster, and with the component S_{Tz} of the total spin along $\mathbf{B}$. The eigenstates may therefore be written as $|S_T,S_{Tz},\alpha\rangle$, where α stands for all other other quantum numbers (if there are any), in addition to S_T and S_{Tz}.[3] The last MST from clusters of type c involves a level crossing of an eigenstate with $S_{Tz}=S_T=n_cS$, called state $|I\rangle$, and the lowest-energy eigenstate with $S_{Tz}=n_cS-1$, called state $|II\rangle$. It can be shown that state $|II\rangle$ must have a total spin $S_T=n_cS-1$.

All the eigenstates states $|S_T,S_{Tz},\alpha\rangle$ may be expressed as linear combinations of the states $|M_1M_2\ldots M_{n_c}\rangle$ in which the magnitude of each individual spin S^i is S, and its z-component is M_i. For the eigenstate $|I\rangle$, with the maximum possible S_{Tz}, all the M_i's must be equal to S,

$$|I\rangle=|SS\ldots S\rangle. \tag{C3}$$

The exchange energy of this eigenstate may be evaluated by noting that

$$2\mathbf{S}^k\cdot\mathbf{S}^l=2S_z^kS_z^l+S_+^kS_-^l+S_-^kS_+^l, \tag{C4}$$

where $S_\pm$ are the raising and lowering operators, and that for the states $|S,M\rangle$ of the individual spins

$$S_\pm|S,M\rangle=\sqrt{(S\mp M)(S\pm M+1)}|S,M\pm1\rangle. \tag{C5}$$

Applying these relations to the exchange Hamiltonian, Eq. (C1), the exchange energy of the eigenstate $|I\rangle$ is

$$E_x(I)=2|J_1|S^2\sum_{\langle k,l\rangle}j_{kl}, \tag{C6}$$

where the sum is on all pairs $\langle k,l\rangle$. This sum is equal to the number or NN pairs in the cluster. The total energy of this state, including the Zeeman term, is

$$E(I)=2|J_1|S^2\sum_{\langle k,l\rangle}j_{kl}-g\mu_{\mathrm{B}}Bn_cS. \tag{C7}$$

In general, there are n_c eigenstates $|S_T,S_{Tz},\alpha\rangle$ for which $S_{Tz}=n_cS-1$. All of them are linear combinations of states $|t\rangle$ in which $M_t=S-1$ and all the other M_i's are equal to S,

$$|t\rangle=|M_1=M_2=\cdots=S,M_t=S-1,\ldots,M_{n_c}=S\rangle. \tag{C8}$$

The action of a term $2\mathbf{S}^k\cdot\mathbf{S}^l$ on each of the states $|t\rangle$ depends on whether t is equal to k, is equal to l, or is different from both k and l. The results for the three cases are

$$2\mathbf{S}^k\cdot\mathbf{S}^l|k\rangle=2S(S-1)|k\rangle+2S|l\rangle, \tag{C9a}$$

$$2\mathbf{S}^k\cdot\mathbf{S}^l|l\rangle=2S(S-1)|l\rangle+2S|k\rangle, \tag{C9b}$$

$$2\mathbf{S}^k\cdot\mathbf{S}^l|t\neq k,l\rangle=2S^2|t\rangle. \tag{C9c}$$

These three equations can be written compactly as

$$2\mathbf{S}^k\cdot\mathbf{S}^l|t\rangle=2S^2|t\rangle-2S(\delta_{tk}+\delta_{tl})|t\rangle+2S\delta_{tk}|l\rangle+2S\delta_{tl}|k\rangle. \tag{C10}$$

Using this expression, the matrix elements of the exchange Hamiltonian given by Eq. (C1), in the subspace spanned by the states $|t\rangle$, are

$$\langle t'|\mathcal{H}_{c,x}|t\rangle=2|J_1|S^2\delta_{t't}\sum_{\langle k,l\rangle}j_{kl}-2|J_1|S\Lambda_{t't}, \tag{C11}$$

where $\Lambda_{t't}$ are the elements of the $n_c\times n_c$ symmetric matrix $\mathbf{\Lambda}$ given by

$$\Lambda_{t't}=\delta_{t't}\sum_k j_{tk}-j_{t't}. \tag{C12}$$

Each diagonal term Λ_{tt} is the number of NN's of spin No. t. Because all these numbers are positive, the trace of the matrix is positive. The off diagonal terms, $-j_{t't}$, are either 0 or -1. Notice that the matrix $\mathbf{\Lambda}$ is independent of the magnitude S of the individual spins.

In Eq. (C11) for $\langle t'|\mathcal{H}_{c,x}|t\rangle$, the first contribution to any diagonal term is equal to the exchange energy $E_x(I)$ of eigenstate $|I\rangle$, given by Eq. (C6). The n_c eigenvalues of the matrix $\langle t'|\mathcal{H}_{c,x}|t\rangle$ can therefore be written as

$$(E_x)_i=E_x(I)-2S|J_1|\lambda_i \tag{C13}$$

where λ_i are the eigenvalues of $\mathbf{\Lambda}$. The eigenstate $|II\rangle$ is the eigenstate with the maximum value of λ_i:

$$\lambda_{\max}=\max(\lambda_i)>0. \tag{C14}$$

Because the trace of the matrix $\mathbf{\Lambda}$ is positive, the sum of the eigenvalues λ_i is positive, so that $\lambda_{\max}$ must be positive. The exchange energy of $|II\rangle$ is then

$$E_x(II)=E_x(I)-2S|J_1|\lambda_{\max}, \tag{C15}$$

which is lower than $E_x(I)$.

The last magnetization step occurs at a field $B_s(c)$ that is determined by the level crossing

$$E_x(I)-g\mu_{\mathrm{B}}B_s(n_cS)=E_x(II)-g\mu_{\mathrm{B}}B_s(n_cS-1), \tag{C16}$$

which gives the reduced field

$$b_s(c) = B_s(c)/g\mu_B|J_1| = 2S\lambda_{max}. \quad \text{(C17)}$$

Because the matrix $\mathbf{\Lambda}$ is independent of S, all its eigenvalues λ_i, including λ_{max}, are independent of S. Thus, in the J_1-model b_s(c) is proportional to S.

For a given cluster type c, the matrix $\mathbf{\Lambda}$ is constructed from the set of j_{kl} values, which may be obtained from the bond list. The maximum eigenvalue of this matrix, λ_{max}, is then used to obtain $b_s(c)$.

As an example, consider a cluster of type 4*A* in Fig. 3. The bond list {110;01;0} gives a $\mathbf{\Lambda}$ matrix

$$\mathbf{\Lambda} = \begin{pmatrix} 2 & -1 & -1 & 0 \\ -1 & 2 & 0 & -1 \\ -1 & 0 & 1 & 0 \\ 0 & -1 & 0 & 1 \end{pmatrix} \quad \text{(C18)}$$

with eigenvalues $\lambda = 0$, $(2-\sqrt{2})$, 2, and $(2+\sqrt{2})$. The largest eigenvalue, $\lambda_{max} = 2+\sqrt{2}$, gives $b_s(4A) = 5(2+\sqrt{2}) \approx 17.071$ for $S = 5/2$, in agreement with the highest b_n in Table II for cluster type 4*A*.

*Electronic address: vbindilatti@if.usp.br
†Electronic address: yshapira@granite.tufts.edu

[1] J. C. Bonner and M. E. Fisher, Phys. Rev. **135**, A640 (1964).
[2] For a review of early works on MST's in diluted magnetic semiconductors, see Y. Shapira, J. Appl. Phys. **67**, 5090 (1990).
[3] For a recent review of MST's, see Y. Shapira and V. Bindilatti, J. Appl. Phys. **92**, 4155 (2002). This review is accompanied by electronically accessible tables for the relevant cluster statistics in the fcc and hcp structures [see EPAPS Document No. E-JAPIAU-92-110220. This document can be received via a direct link in the online article's HTML reference section or via the EPAPS homepage(http://www.aip.org/pubservs/epaps.html).].
[4] Some of the works in molecular crystals are reviewed by D. Gatteschi and R. Sessoli, in *Magnetism: Molecules to Materials III*, edited by J. S. Miller and M. Drillon (Wiley-VCH, Weinheim, 2002), Chap. 3, pp. 63–108.
[5] J. R. Friedman, M. P. Sarachik, J. Tejada, and R. Ziolo, Phys. Rev. Lett. **76**, 3830 (1996).
[6] L. Thomas, F. Lionti, R. Ballou, D. Gatteschi, R. Sessoli, and B. Barbara, Nature (London) **383**, 145 (1996).
[7] E. M. Chudnovsky and J. Tejada, *Macroscopic Quantum Tunneling of the Magnetic Moment* (Cambridge, New York, 1998).
[8] A. Paduan-Filho, N. F. Oliveira, Jr., V. Bindilatti, S. Foner, and Y. Shapira, Phys. Rev. B **68**, 224417 (2003), and references therein.
[9] S. A. Crooker, N. Samarth, and D. D. Awschalom, Phys. Rev. B **61**, 1736 (2000). This work contains results for cluster statistics in the NN cluster model, for clusters with up to three spins.
[10] A. Paduan-Filho, X. Gratens, V. Bindilatti, N. F. Oliveira, Jr., and Y. Shapira, following paper, Phys. Rev. B **72**, 064415 (2005).
[11] X. Gratens, V. Bindilatti, N. F. Oliveira, Jr., Y. Shapira, S. Foner, Z. Golacki, and T. E. Haas, Phys. Rev. B **69**, 125209 (2004).
[12] The choice of x as the fraction of cations that are magnetic is traditional in the area of diluted magnetic semiconductors. Many papers on the statistics of cluster types also use this notation. However, in many other papers the fraction of cations that are magnetic is designated as p, instead of x, and the nonmagnetic fraction is designated as q instead of $(1-x)$.
[13] D. Stauffer and A. Aharony, *Introduction to Percolation Theory*, Revised 2nd ed. (Taylor & Francis, London, 1994).
[14] V. Bindilatti (unpublished).
[15] For the three cluster models that are considered, the numbering of the spins in Fig. 2 satisfies the hierarchy in Ref. 14. The spins numbered as 2 and 3 are of equal rank in this hierarchy. Interchanging their numbers does not change the bond list.
[16] See EPAPS Document No. E-PRBMDO-72-001525 for electronically-accessible tables for the J_1-model in the square, lattice, which give relevant information for all cluster types with sizes $n_c \leqslant 12$. For each cluster type, these tables give the bond list, the perimeter polynomial, the spontaneous total spin, and the reduced saturation field at $T=0$. This document can be received via a direct link in the online article's HTML reference section or via the EPAPS homepage(http://www.aip.org/pubservs/epaps.html).
[17] M. F. Sykes and M. Glen, J. Phys. A **9**, 87 (1976).
[18] Several papers on the statistics of cluster types are cited in Ref. 3. The earliest known to us is R. E. Behringer, J. Chem. Phys. **29**, 537 (1958).
[19] The alternative is to give the statistical parameters in Eq. (4) for more than 80 000 individual configurations.
[20] Individual clusters may not be considered as independent in calculations of some nonequilibrium properties, including spin relaxation. The reason is that weak intercluster interactions are central to some nonequilibrium processes, even when they have only a very minor influence on the equilibrium properties. An example is the process of cross relaxation, which involves clusters of different types.
[21] Many of these results are taken from X. Gratens, V. Bindilatti, E. ter Haar, N. F. Oliveira, Jr., Y. Shapira, and F. C. Montenegro, Phys. Rev. B **64**, 214424 (2001). The quartet types 4*A*, 4*B*, and 4*C* in Fig. 3 of the present paper correspond to quartet types 1, 3, and 2 of that reference, respectively. The quintet types 5*A*, 5*B*, 5*C*, and 5*D* in the same Fig. 3 correspond to quintet types 2, 4, 3, and 5, respectively.
[22] The term "non-negligible size" may be quantified. In the theory, a minimum size, say, 0.1% of m_s, may be specified. Experimentally, any MST which is resolved may be considered as having a non-negligible size.